Proc. NIPR Symp. Antarct. Geosci., 4, 22–40, 1990

A STAUROLITE-BEARING CORUNDUM-GARNET GNEISS FROM THE EASTERN SØR RONDANE MOUNTAINS, ANTARCTICA

Masao ASAMI[1], Edward S. GREW[2] and Hiroshi MAKIMOTO[3]

[1]*Department of Geological Sciences, College of Liberal Arts, Okayama University, 2-1, Tsushima Naka 2-chome, Okayama 700*
[2]*Department of Geological Sciences, University of Maine, 110 Boardman Hall, Orono, Maine 04469, U.S.A.*
[3]*Geological Survey of Japan, 1-3, Higashi 1-chome, Tsukuba 305*

Abstract: Staurolite is found as inclusions in garnet in a corundum-garnet gneiss from an outcrop of two-pyroxene gneiss in the eastern Sør Rondane Mountains. The staurolite is a zinc-poor variety of normal iron content (ZnO=0.10–0.32 wt%; X_{Fe}=0.74–0.80), and occurs only in 'domains', consisting mainly of plagioclase, enclosed in the zoned garnet with magnesian cores (X_{Fe}=0.69–0.70). From textural and mineralogical observations, it is possible to distinguish (1) a staurolite-bearing mineral association in the domains and (2) a granulite-facies association of the garnet core with the matrix constituents plagioclase, biotite, sillimanite, corundum, spinel, magnetite and ilmenite. In addition, compositional relations between staurolite and the association garnet-corundum-spinel-sillimanite is consistent with the prograde reaction staurolite=garnet+corundum+spinel +sillimanite+H_2O. On the basis of textural features and paragenetic relations, staurolite in this gneiss is interpreted to be a relic that was isolated from the matrix by growing of garnet in a prograde metamorphic process attaining the granulite facies. A later, probably amphibolite-facies metamorphic episode is suggested by Fe-Mg redistribution between garnet and biotite in direct contact.

1. Introduction

Staurolite relatively rich in iron (Fe/(Fe+Mg)>0.7) is a common constituent in medium-grade regional metamorphic rocks of pelitic composition (DEER *et al.*, 1982). Formation of staurolite under conditions of the middle amphibolite facies is consistent with the results of experimental studies on staurolite stability (RICHARDSON, 1968; HOSCHEK, 1969; GANGULY, 1972; RAO and JOHANNES, 1979). In rare cases staurolite is also found in pelitic rocks from upper amphibolite- and granulite-facies metamorphic terrains, but it appears to be restricted to relics or to varieties enriched in additional cations such as zinc and titanium (ASHWORTH, 1975; HIROI *et al.*, 1983; MOTOYOSHI *et al.*, 1985; MOTOYOSHI, 1986; SHIRAISHI, 1986; HIROI and KISHI, 1989a, b).

The eastern Sør Rondane Mountains in the East Antarctic shield are underlain by a migmatized gneissic complex consisting mainly of upper amphibolite- to granulite-facies metamorphic rocks (ASAMI *et al.*, 1989; GREW *et al.*, 1989). In the course of our petrological study of the metamorphic rocks, staurolite was found in a corundum-garnet gneiss collected from the southeastern part of this area. This is the first finding of

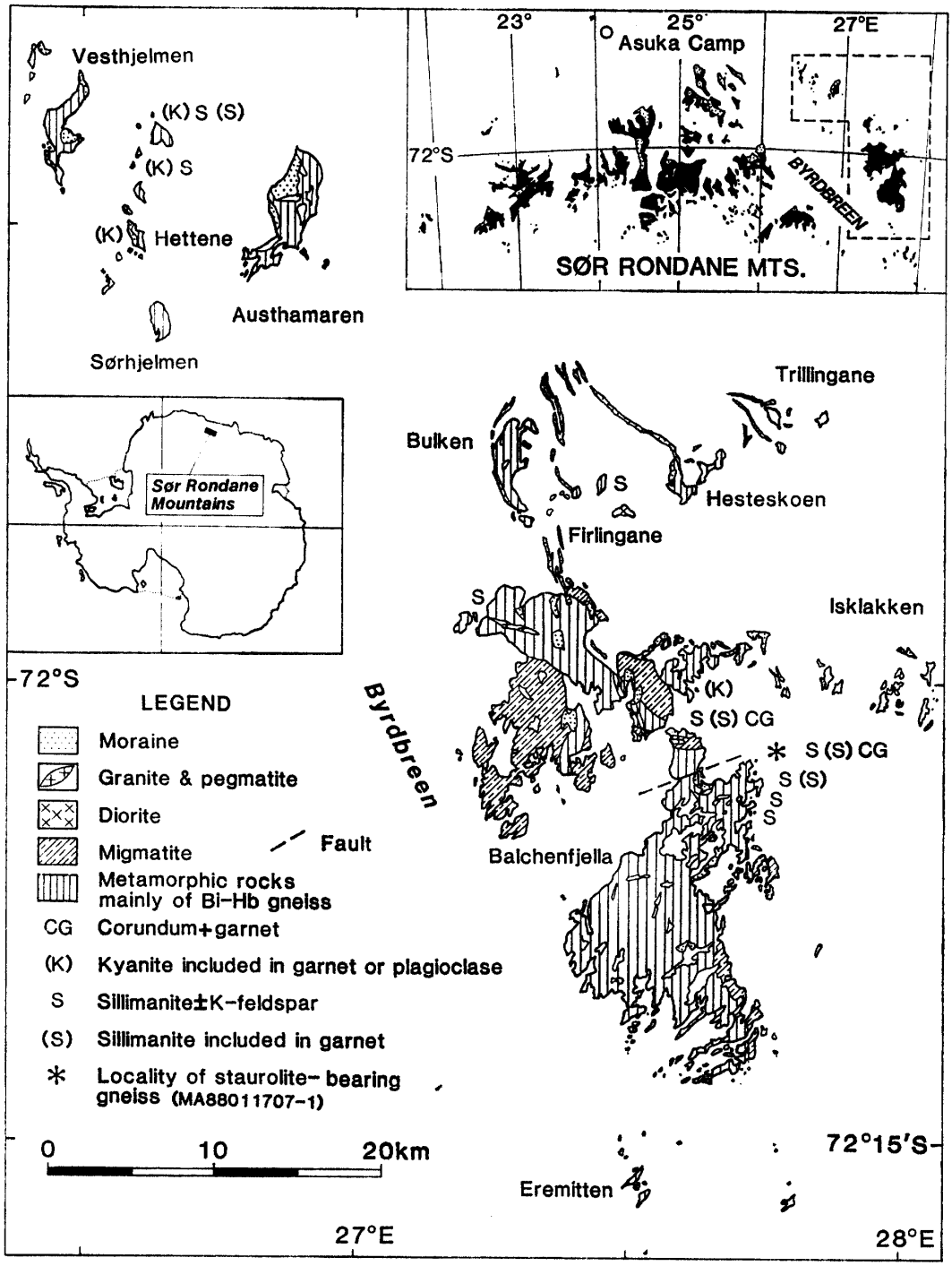

Fig. 1. Simplified geological map of the eastern Sør Rondane Mountains, showing localities of the staurolite-bearing gneiss (MA88011707-1) and some characteristic minerals. Modified from Fig. 1 in ASAMI *et al. (1989).*

staurolite in the Sør Rondane Mountains. Petrographic characters and mineral chemistry of the staurolite-bearing gneiss are described in this paper.

2. Geological Setting

The eastern Sør Rondane Mountains (71°40′–72°20′S, 26°30′–28°E) in East Queen Maud Land was geologically surveyed by us during JARE-29, and our geological and preliminary petrological studies have been published (ASAMI *et al.*, 1989; GREW *et al.*, 1988, 1989). The surveyed exposures are composed of gneissic rocks accompanied by migmatite and small intrusive bodies of granite, pegmatite and diorite (Fig. 1). A late Ordovician plutonic activity is suggested by a 450 Ma Rb-Sr biotite age for pegmatite from Trillingane (VAN AUTENBOER, 1969). The metamorphic rocks are presumed to be dominantly of sedimentary and volcanogenic origin (seven rock types) and to a lesser extent of magmatic origin (five rock types) (ASAMI *et al.*, 1989). Geological structure of the metamorphic rocks is complex due to the "combined" effects of folding and migmatization. According to ASAMI *et al.* (1989), GREW *et al.* (1989) and MAKIMOTO *et al.* (1990), it is suggested that upper amphibolite to hornblende granulite-facies metamorphism was followed by an amphibolite-facies event, which is closely related with the migmatization.

3. Mode of Occurrence

The dominant rock type of the metamorphic rocks is biotite-hornblende gneiss, in which layers of garnet-biotite gneiss and biotite gneiss are locally intercalated. The garnet-biotite gneiss contains sillimanite and rarely kyanite or corundum (Fig. 1). In addition to the localities reported by GREW *et al.* (1989), kyanite has been found in garnet and plagioclase of a garnet-biotite gneiss (HM88012805D) from Hettene. The staurolite-bearing corundum-garnet gneiss (MA88011707–1) of primary concern in the present paper was collected at the northeastern end of southern Balchenfjella (Fig. 1), one of the two localities for corundum-garnet gneiss.

The staurolite-bearing gneiss is part of a sillimanite-garnet-biotite gneiss layer about 3 m thick between two layers of quartzo-feldspathic biotite-hornblende gneiss. These layers are part of a concordant layered sequence of biotite-hornblende and hornblende gneisses with orthopyroxene and of sillimanite-garnet-biotite gneiss.

4. Petrography

The staurolite-bearing gneiss is dark gray due to abundant biotite. Wine-red garnet porphyroblasts, up to several millimeters in diameter, are scattered in a medium-grained gneissose matrix. Locally, white lenses and bands, a few to several millimeters thick, of plagioclase aggregates are formed parallel or subparallel to the gneissosity. Prisms and needles of sillimanite are visible on the gneissosity planes defined by flattened aggregates of biotite in parallel orientation.

Under the microscope, no quartz was found, and porphyroblasts of garnet (Ga) are developed in a matrix consisting of plagioclase (Pl), biotite (Bi), sillimanite (Sil),

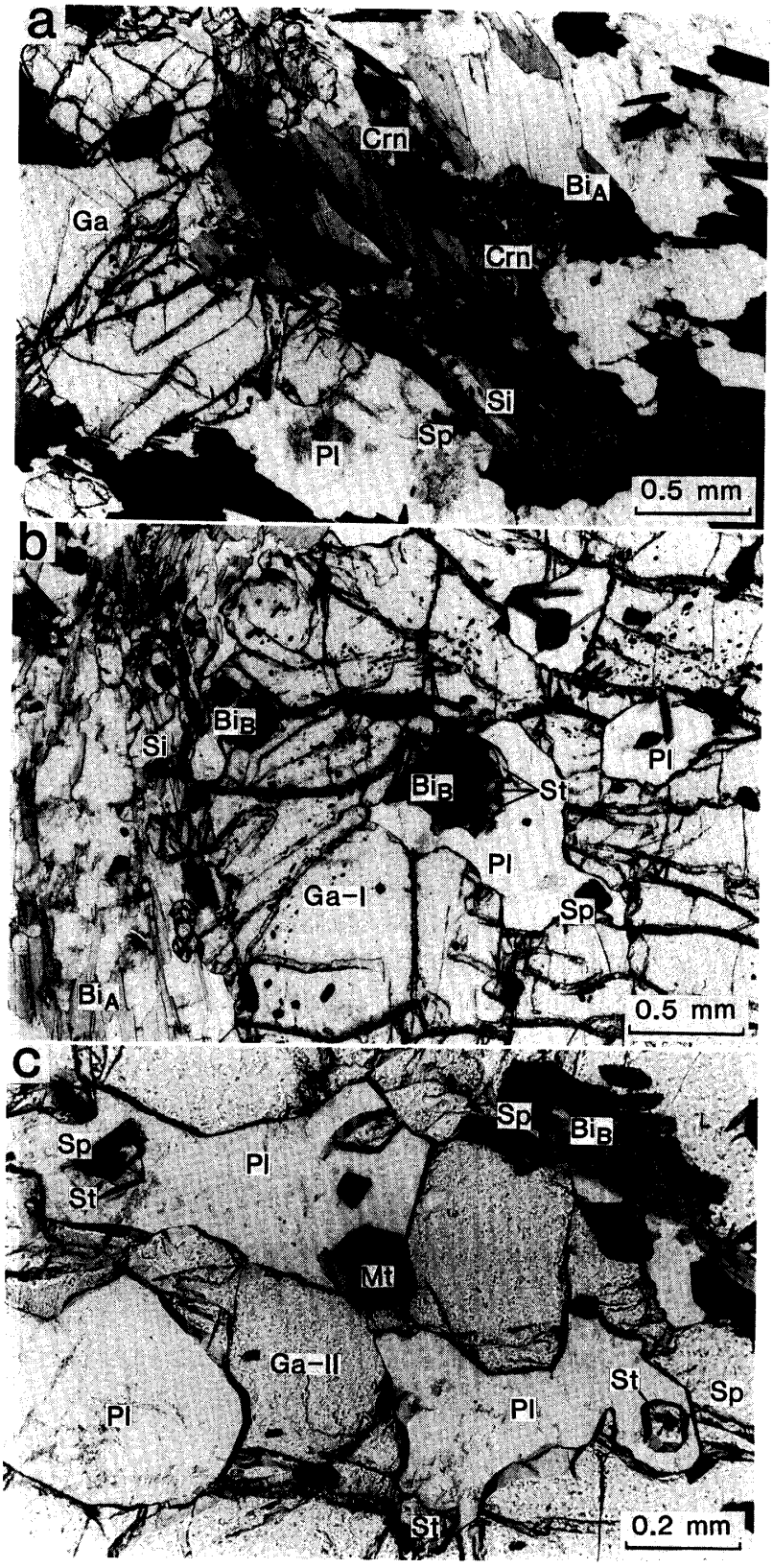

a. A garnet porphyroblast (Ga) and surrounding gneissose matrix consisting of plagioclase (Pl), Type-A biotite (Bi_A), sillimanite (Si), corundum (Crn), spinel (Sp), magnetite and ilmenite. One nicol.

b. A garnet porphyroblast (Ga-I) with relatively large inclusions, 'domain', of plagioclase (Pl). In a domain (center), small subhedral grains of staurolite (St) are associated with Type-B biotite (Bi_B), spinel (Sp) and ilmenite. A discrete grain of Type-B biotite is also found. Si: matrix sillimanite; Bi_A: Type-A biotite. One nicol.

c. Domains (Pl) in a garnet porphyroblast (Ga-II). Three grains of staurolite (St) are found in the domains: one (upper left) interlocks with spinel (Sp), another (lower right) includes spinel and the other (bottom) is partially embedded in garnet. Bi_B: Type-B biotite; Mt: magnetite. One nicol.

Fig. 2. Photomicrographs of the staurolite-bearing gneiss.

corundum (Crn), spinel (Sp), magnetite (Mt), ilmenite (Il) and zircon (Fig. 2a). Biotite, plagioclase, sillimanite, spinel, magnetite, ilmenite and zircon are also included in garnet. Each included mineral usually occurs as discrete grains or prisms up to 0.3 mm across or long. But some inclusions of plagioclase form somewhat larger grains or aggregates, 0.4 to 1.3 mm across, that are accompanied by biotite, spinel and ilmenite. In this paper such inclusions are referred to as 'domains' in order to distinguish them from the discrete grains.

Several textural types of biotite are distinguished as follows: (A) flakes in the matrix, (A') matrix biotite flakes in contact with garnet, and (B) grains or small flakes included in garnet (Fig. 2b). All types of biotite show the almost same pleochroism: X-pale brownish yellow and Y- and Z-yellowish brown. In addition, tiny flakes of biotite with weak pleochroism, X-colorless; Y- and Z-pale green, rarely occur between garnet and plagioclase.

Staurolite (St) is found in a few domains in garnet porphyroblasts, but has not been found in the matrix (Fig. 2b, c). It forms small euhedral or subhedral grains less than 0.2 mm in diameter as follows: (1) largely enclosed by Type-B biotite (Fig. 2b), (2) included in plagioclase (Fig. 2c) and (3) partially enclosed by garnet (Fig. 2c). Staurolite is rarely intergrown with or includes spinel (Fig. 2c). Mineral associations observed in the staurolite-bearing domains are St+Sp+Ga+Bi+Pl±Il±Mt and St+Sp+Ga+Pl. The staurolite shows weak pleochroism, X- and Y-colorless to very pale yellow; Z-pale straw yellow, with $2Vz=84^\circ$ and $r>v$ (moderate) (measured by Leitz five-axis universal stage).

Plagioclase rarely shows optical zoning. Plagioclase in the matrix and in the domains enclosed in garnet cannot be distinguished optically from one another.

Spinel is deep green and many grains of spinel include opaque dust, which is possibly magnetite. Spinel is also included in sillimanite and rarely staurolite (Fig. 2c). Corundum is colorless and occurs as anhedral or subhedral grains. Both minerals are scattered in the matrix and are in contact with all the other matrix constituents including garnet (Fig. 2a).

Sillimanite is not only intimately associated with biotite in the matrix, but also is in contact with all the other constituents (Fig. 2a, b).

5. Chemical Compositions of Minerals

Chemical analyses were made of garnet, biotite, staurolite, spinel, plagioclase, corundum, sillimanite and ore minerals, using the JEOL JXA-733 electronprobe micro-analyzer and the Bence-Albee correction method. Two or more grains of each mineral per thin section were examined. Representative individual analyses are listed in Tables 1 to 5.

5. 1. Garnet

Compositional profiles were obtained on two garnet porphyroblasts, Ga-I and Ga-II, both profiles extend from edges in contact with plagioclase to edges in contact with matrix biotite of Type A′ (Fig. 3 and Table 1). The profile of Ga-I crosses a plagioclase aggregate (domain 1), which contains biotite, staurolite, spinel and ilmenite,

while the profile of Ga-II crosses a plagioclase grain and two spinel grains.

Figures 3a and 3b show distinct outward increases of X_{Fe} (=Fe/(Fe+Mg)) as a result of increasing Fe and decreasing Mg contents towards the edges. Mn content also increases towards the edge, although the Mn and Ca contents are low throughout the garnets. These outward increases are more marked towards the edges in contact with biotite than towards the edges in contact with plagioclase. In contrast to the edges, the interiors of both garnets are relatively magnesian (X_{Fe}=0.69 and 0.70 at the cores of Ga-I and Ga-II, respectively). Moreover, the profile across interior of Ga-I, which is larger than Ga-II, is flat, implying a relatively homogeneous composition. No compositional variation is observed near the contacts with inclusions of plagioclase

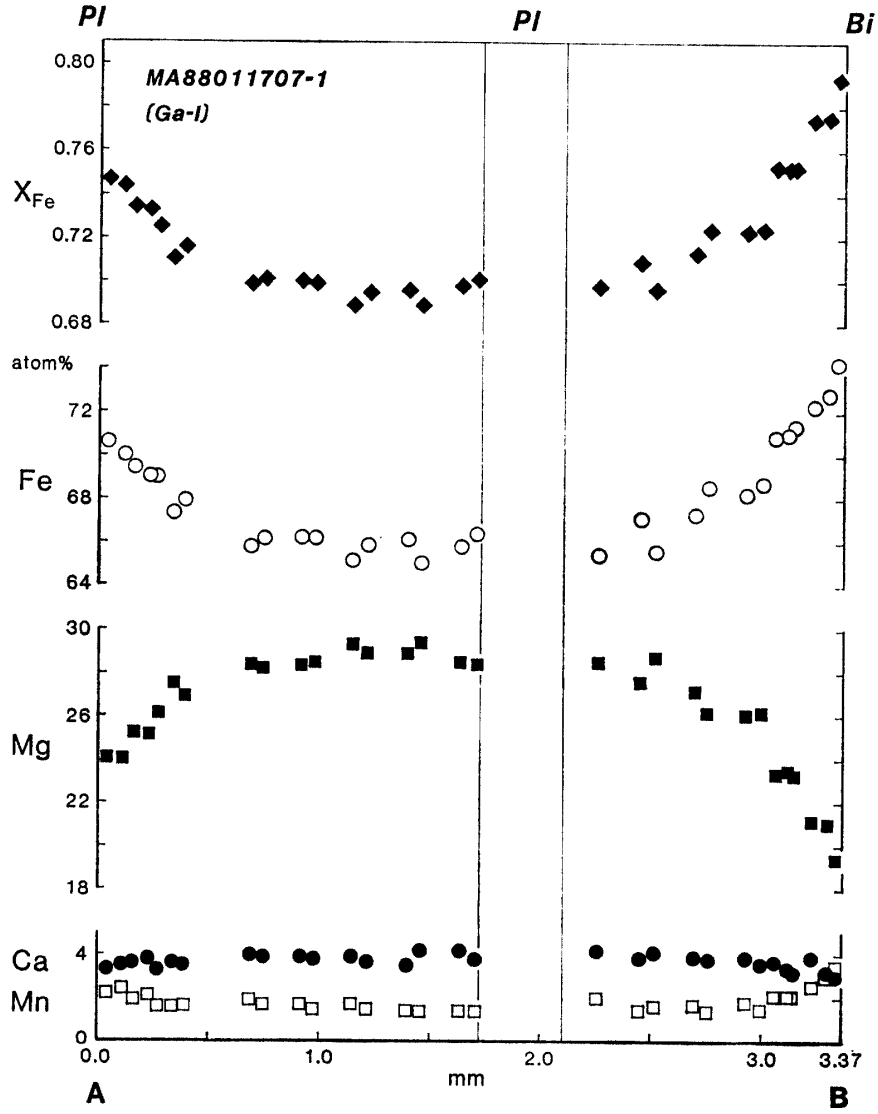

Fig. 3. Compositional profiles of garnet porphyroblasts.
(a) Ga-I. Biotite contacts at edge B.
Abbreviations: Bi—biotite, Pl—plagioclase.

and spinel in either garnet. These compositional features suggest that the magnesian compositions resulted from equilibration during the main metamorphic phase, whereas the Fe-enrichment took place mainly through retrograde Fe-Mg exchange between garnet edges and biotite in direct contact or nearby in the matrix.

Garnet in contact with Type-B biotite (I_{Bil-3}, Table 1) is higher in X_{Fe} than average core garnet (C_I, Table 1). Garnet in contact with staurolite (I_{St}) is also more iron-rich than typical core garnet (C_{II}) although still slightly more magnesian ($X_{Fe}=0.72$) than the contacting staurolite ($X_{Fe}=0.74$), the reverse relation to that reported by ALBEE (1972). Such reversals between garnet and staurolite have been reported: *e.g.*, RICE (1985); GREW and SANDIFORD (1985); HIROI (1987); BALLEVRE *et al.* (1989).

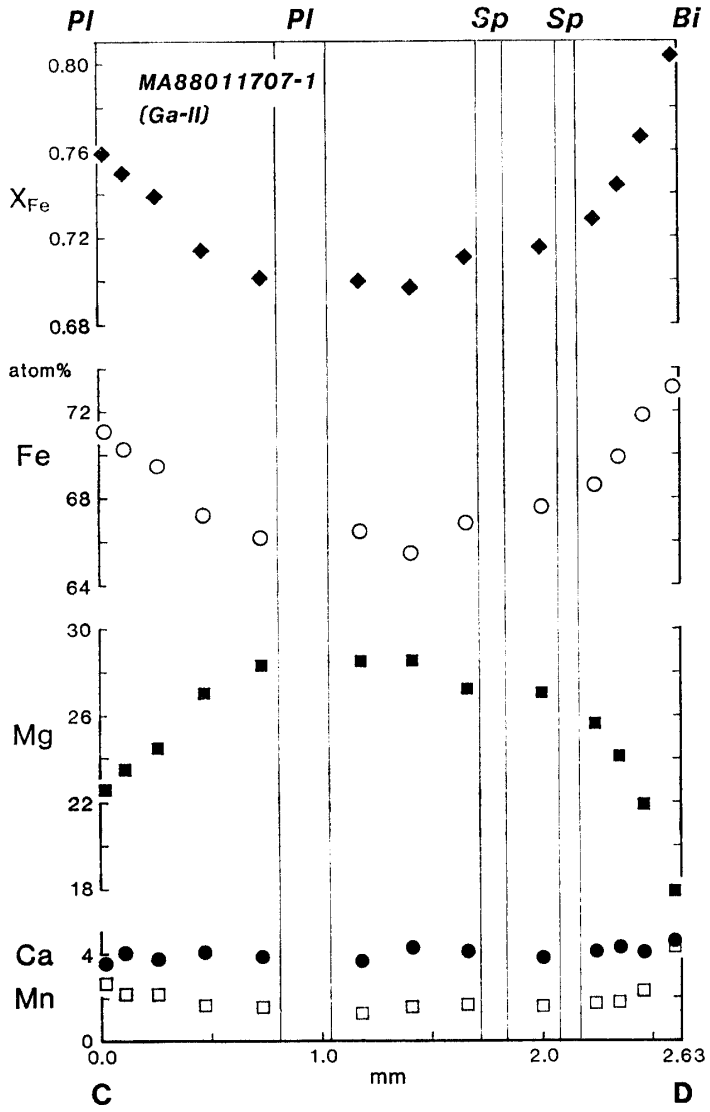

Fig. 3. Compositional profiles of garnet porphyroblasts. (b) Ga-II. Biotite contacts at edge D. Abbreviations: Bi—biotite, Pl—plagioclase, Sp—spinel.

Table 1. Representative microprobe analyses of garnet.

	Ga-I						Ga-II			
Anal. No.	C_I 42	E_A 48	E_B 20	I_{BI1} 39	I_{BI2} 63′	I_{BI3} 17	C_{II} 79	E_C 87	E_D 69	I_{St} 105
SiO_2	38.00	38.65	37.68	38.66	38.72	37.18	38.29	38.12	37.94	38.26
TiO_2	0.00	0.01	0.02	0.00	0.05	0.00	0.00	0.00	0.07	0.00
Al_2O_3	21.52	21.00	20.94	21.19	21.77	20.78	21.79	21.09	21.29	20.54
Cr_2O_3	0.00	0.00	0.00	0.03	0.00	0.00	0.00	0.05	0.05	0.07
FeO*	30.57	33.13	33.97	31.56	31.51	33.68	30.92	33.01	32.67	31.48
MnO	0.80	1.00	1.57	0.68	0.78	1.40	0.76	1.26	1.93	0.96
MgO	7.73	6.31	4.99	6.79	6.64	4.93	7.56	5.88	4.49	6.95
ZnO	—	—	—	—	0.00	0.00	0.10	—	0.00	0.05
CaO	1.42	1.20	1.06	1.34	1.38	1.22	1.59	1.32	1.59	1.33
Na_2O	0.05	0.01	0.00	0.00	0.05	0.00	0.00	0.00	0.04	0.00
K_2O	0.00	0.00	0.01	0.00	0.00	0.00	0.00	0.01	0.01	0.00
Total	100.09	101.31	100.24	100.25	100.90	99.19	101.01	100.74	100.08	99.64
					24 (O)					
Si	5.946	6.035	6.000	6.051	6.017	5.984	5.942	6.001	6.027	6.046
Al	3.969	3.865	3.930	3.909	3.988	3.942	3.986	3.914	3.986	3.826
Ti	0.000	0.001	0.002	0.000	0.000	0.000	0.000	0.000	0.008	0.000
Cr	0.000	0.000	0.000	0.004	0.000	0.000	0.000	0.006	0.006	0.009
Fe	4.000	4.327	4.524	4.131	4.095	4.534	4.013	4.346	4.340	4.160
Mn	0.106	0.132	0.212	0.090	0.103	0.191	0.100	0.168	0.260	0.128
Mg	1.803	1.468	1.184	1.584	1.538	1.183	1.748	1.380	1.063	1.637
Zn	—	—	—	—	0.000	0.000	0.011	—	0.000	0.006
Ca	0.238	0.201	0.181	0.225	0.230	0.210	0.264	0.223	0.271	0.225
Na	0.015	0.003	0.000	0.000	0.015	0.000	0.000	0.000	0.012	0.000
K	0.000	0.000	0.002	0.000	0.000	0.000	0.000	0.002	0.002	0.000
Alm	65.1	70.6	74.2	68.5	68.6	74.1	65.5	71.1	73.1	67.6
Pyr	29.3	24.0	19.4	26.3	25.8	19.3	28.5	22.6	17.9	26.6
Spe	1.7	2.2	3.5	1.5	1.7	3.1	1.6	2.7	4.4	2.1
Gro	3.9	3.3	3.0	3.7	3.9	3.4	4.3	3.6	4.6	3.7
X_{Fe}	0.689	0.747	0.793	0.723	0.727	0.793	0.697	0.759	0.803	0.718

* Total iron as FeO. X_{Fe}=Fe/(Fe+Mg). C_I, C_{II}: cores of Ga-I and Ga-II; E_{A-D}: edges A, B, C, D. I_{BI}, I_{St}: interiors contacting with Type-B biotite and staurolite, respectively.

5.2. *Biotite*

Fourteen flakes of Type-A, three flakes of Type-A′, and three Type-B biotites in Ga-I, two flakes from the staurolite-bearing domains and a discrete grain, were analyzed together with a flake of pale green biotite from domain 1 in Ga-II (selected analyses in Table 2).

Figure 4 shows that Type-A biotites are higher in X_{Fe} and Ti content than Type-B biotites from the staurolite-bearing domains. Type-B biotite occurring as discrete inclusions is also as high in both compositional features as Type A. On the other hand, Type-A′ biotites are somewhat lower in X_{Fe} and Ti content than Type-A biotites. The pale green biotite is magnesian and extremely low in Ti content. In Fig. 4, a correlation between X_{Fe} and Ti content, as well as the inverse relation between X_{Fe} and Si content

Table 2. Representative microprobe analyses of biotite.

	Type A		Type A′		Type B			
	Bi_1	Bi_2	Bi_3	Bi_4	Bi_5	Bi_6	Bi_7	Bi_8
	>I	>II	/IE_B	/IIE_D	/I_{BI1}	/I_{BI2}	/I_{BI3}	PG-Bi
Anal. No.	2	91	6	68	38	62′	16	107
SiO_2	34.88	34.48	35.12	34.75	35.60	35.41	34.62	37.16
TiO_2	3.15	3.20	1.72	2.71	2.40	2.66	2.88	0.31
Al_2O_3	18.48	18.82	18.95	19.60	18.47	18.45	18.62	20.14
Cr_2O_3	0.03	0.02	0.00	0.03	0.04	0.05	0.05	0.02
FeO*	18.38	18.44	17.04	18.42	14.47	14.07	17.97	11.58
MnO	0.06	0.02	0.00	0.12	0.00	0.02	0.01	0.00
MgO	9.94	10.20	11.69	10.41	13.86	14.10	10.85	17.08
ZnO	0.00	0.05	0.00	0.00	—	0.00	0.00	0.04
CaO	0.03	0.00	0.01	0.00	0.00	0.01	0.01	0.23
Na_2O	0.29	0.27	0.26	0.24	0.32	0.43	0.32	0.41
K_2O	8.11	8.61	8.53	8.86	8.73	8.55	8.45	8.06
Total	93.35	94.11	93.32	95.14	93.89	93.75	93.78	95.03
				22 (O)				
Si	5.369	5.286	5.376	5.266	5.359	5.329	5.309	5.401
Al	3.353	3.401	3.419	3.501	3.277	3.273	3.365	3.450
Ti	0.365	0.369	0.198	0.309	0.272	0.301	0.332	0.034
Cr	0.004	0.002	0.000	0.004	0.005	0.006	0.006	0.002
Fe	2.366	2.364	2.182	2.335	1.822	1.771	2.305	1.408
Mn	0.008	0.003	0.000	0.015	0.000	0.003	0.001	0.000
Mg	2.280	2.330	2.667	2.351	3.109	3.163	2.480	3.700
Zn	0.000	0.006	0.000	0.000	—	0.000	0.000	0.004
Ca	0.005	0.000	0.002	0.000	0.000	0.002	0.002	0.036
Na	0.087	0.080	0.077	0.071	0.093	0.125	0.095	0.116
K	1.593	1.684	1.666	1.713	1.677	1.642	1.653	1.494
X_{Fe}	0.509	0.504	0.450	0.498	0.369	0.359	0.482	0.276

* Total iron as FeO. X_{Fe}=Fe/(Fe+Mg). >I: near Ga-I; >II: near Ga-II. /IE_B, /IIE_D, /I_{BI}: contact with edge E_B of Ga-I, edge E_D of Ga-II and interiors of Ga-I, respectively. PG-Bi: pale green biotite.

(Table 2), is a characteristic feature of biotite, which has been discussed by GUIDOTTI *et al.* (1977) and GUIDOTTI (1984).

Mg/Fe ratios of three kinds of mineral pairs, Type-A biotite-garnet core, Type-A′ biotite-contacting garnet edge and Type-B biotite-contacting garnet, are plotted in Fig. 5. The lower K_D values of the first mineral pairs are obviously distinguishable from the higher values of the other two kinds. Such a relation, together with the characteristics of garnet zoning (Fig. 3), suggests that the first pairs represent a higher-temperature association at the main metamorphic stage and the other two kinds a lower-temperature association at a later stage.

The chemical character and mode of occurrence of the pale green biotite suggest that the biotite is a late, low-temperature product compared with the brownish varieties described above.

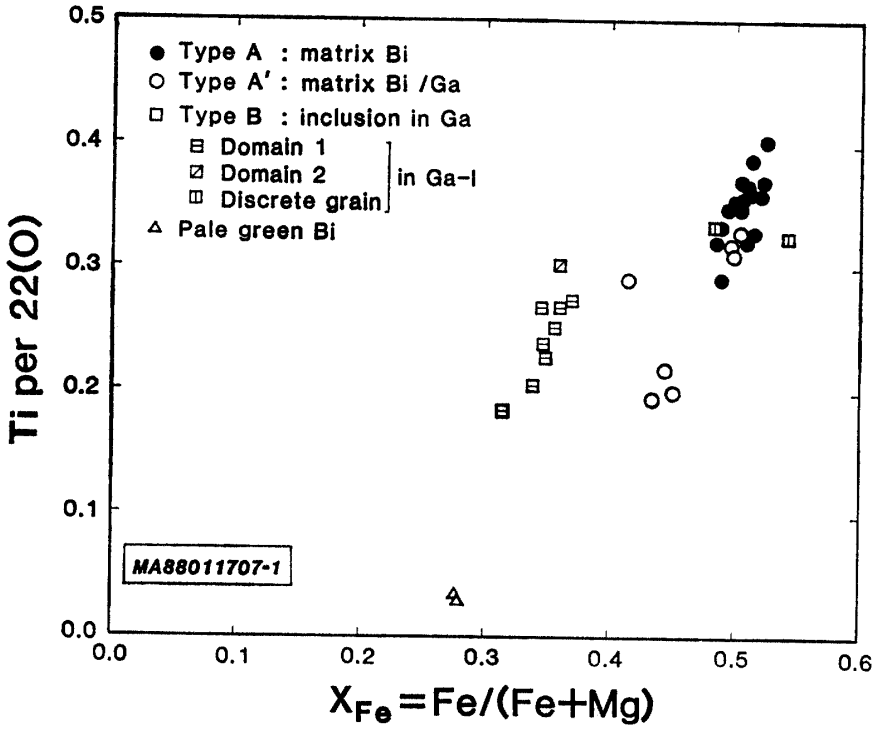

Fig. 4. Ti-X_{Fe} plot of three types of biotite. Compositions of pale green biotite are also shown.

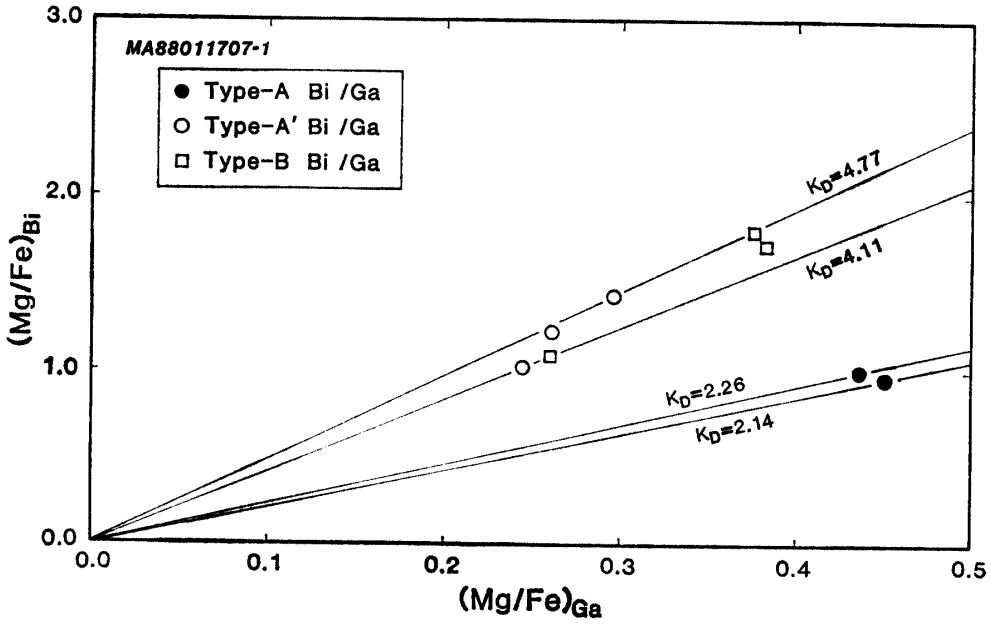

Fig. 5. Mg-Fe distribution between garnet and biotite.

5.3. Staurolite

Eight staurolite grains included in Ga-I and Ga-II were analyzed: three grains from domain 1 and a grain from domain 2 in Ga-I, all contacting with Type-B biotite (Fig. 2b), and two grains from domain 1 and two grains from domain 2 in Ga-II, one contacting with spinel and the other with garnet (Fig. 2c).

Figure 6 and Table 3 show that the staurolites are zinc-poor (ZnO=0.10–0.32 wt%) and have normal iron contents with some variations of X_{Fe} (0.74–0.80). Low TiO_2 contents are also characteristic of the staurolites (0.00–0.67). Among the staurolite grains analyzed, the grains contacting with biotite in Ga-I are slightly higher in X_{Fe} (0.77–0.80) and TiO_2 content (0.56–0.67 wt%) than those contacting with spinel and garnet in Ga-II (X_{Fe}=0.74–0.75 and TiO_2=0.00–0.06 wt%).

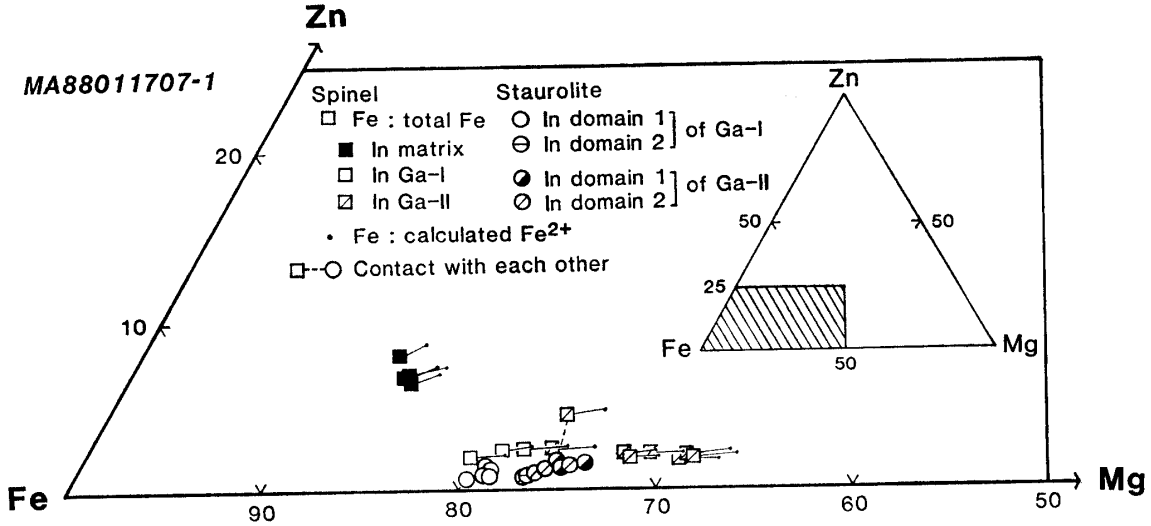

Fig. 6. Zn-Fe-Mg diagram for staurolite and spinel.

5.4. Spinel

Thirteen grains of spinel were analyzed: two grains enclosed in Ga-I, a grain, interlocking with staurolite (Fig. 2c), from domain 1 in Ga-II and six discretely enclosed in Ga-II, and the rest four from the matrix. The analyses are plotted in Fig. 6 and some of them are listed in Table 3.

These analyses show that the spinels are of relatively iron-rich compositions in the spinel-hercynite series with gahnite contents of 1.7–8.7 mole% and estimated Fe^{3+} of 0.099–0.188 per 8 oxygens and 6 cations. Figure 6 shows that the X_{Fe} values for spinel overlap those for staurolite, but have a greater variation (0.66–0.85). In addition, spinels are higher in Zn value than staurolite. Among the spinels, four grains from the matrix are richest in iron and zinc (X_{Fe}=0.83–0.85, ZnO=3.23–4.08 wt%). A spinel in contact with staurolite is more zincic than the other spinels enclosed in garnet, but is similar in X_{Fe} to the contacting staurolite (Sp_3 and St_4 in Table 3).

5.5. Plagioclase

Analyzed plagioclases include ten grains from the matrix and five grains from

Table 3. Representative microprobe analyses of staurolite and spinel.

	Staurolite					Spinel			
	I_1	I_2	II_1		II_2	M	I	II_1	II
	St_1 /Bi_5	St_2 /Bi_6	St_3 /I_{St}	St_4 /Sp_3	St_5 <Pl	Sp_1 /Pl	Sp_2 <Ga	Sp_3 /St_4	Sp_4 <Ga
Anal. No.	30	61	108	109	120	129	60	111	74
SiO_2	25.67	26.73	26.01	26.20	25.73	0.01	0.03	0.01	0.01
TiO_2	0.67	0.59	0.06	0.00	0.10	0.01	0.00	0.00	0.02
Al_2O_3	55.41	55.65	56.16	55.67	57.10	55.49	57.57	57.73	59.09
Cr_2O_3	0.03	0.07	0.08	0.01	0.07	0.55	0.63	0.50	0.28
FeO*	13.12	13.26	12.25	13.01	12.78	35.69	36.20	32.99	31.18
MnO	0.09	0.13	0.00	0.06	0.02	0.17	0.17	0.06	0.12
MgO	1.98	2.26	2.43	2.39	2.44	3.56	5.10	6.02	8.07
ZnO	0.13	0.15	0.28	0.32	0.27	3.40	0.98	2.26	0.98
CaO	0.02	0.01	0.03	0.02	0.00	0.01	0.00	0.01	0.00
Na_2O	0.00	0.00	0.00	0.00	0.02	0.00	0.00	0.00	0.00
K_2O	0.01	0.03	0.01	0.00	0.00	0.00	0.00	0.00	0.00
Total	97.13	98.88	97.31	97.68	98.53	98.89	100.68	99.58	99.75
			46 (O)				8 (O) & 6 cat.		
Si	7.179	7.339	7.225	7.278	7.078	0.001	0.002	0.001	0.001
Al	18.266	18.011	18.387	18.228	18.516	3.785	3.801	3.825	3.840
Ti	0.141	0.122	0.013	0.000	0.021	0.000	0.000	0.000	0.001
Cr	0.007	0.015	0.018	0.002	0.015	0.025	0.028	0.022	0.012
Fe^{3+}**	—	—	—	—	—	0.188	0.168	0.152	0.145
Fe^{2+}	3.069	3.045	2.846	3.023	2.940	1.540	1.527	1.399	1.293
Mn	0.021	0.030	0.000	0.014	0.005	0.008	0.008	0.003	0.006
Mg	0.825	0.925	1.006	0.989	1.000	0.307	0.426	0.504	0.663
Zn	0.027	0.030	0.057	0.066	0.055	0.145	0.041	0.094	0.040
Ca	0.006	0.003	0.009	0.006	0.000	0.001	0.000	0.001	0.000
Na	0.000	0.000	0.000	0.000	0.011	0.000	0.000	0.000	0.000
K	0.004	0.011	0.004	0.000	0.000	0.000	0.000	0.000	0.000
Fe	78.3	76.1	72.8	74.1	73.6	77.3	76.6	70.1	64.8
Mg	21.0	23.1	25.7	24.3	25.0	15.4	21.4	25.3	33.2
Zn	0.7	0.8	1.5	1.6	1.4	7.3	2.0	4.7	2.0
X_{Fe}	0.788	0.767	0.739	0.753	0.746	0.834	0.782	0.735	0.661

* Total iron as FeO. ** Calculated by normalizing to 8 oxygens and 6 cations. $X_{Fe}=Fe^{2+}/(Fe^{2+}+Mg)$. I: in Ga-I; II: in Ga-II. $I_{1,2}$: domains 1 and 2 in Ga-I; $II_{1,2}$: domains 1 and 2 in Ga-II. M: in the matrix. /Bi, /I_{St}, /Pl, /Sp, /St: contact with biotite, garnet interior, plagioclase, spinel and staurolite, respectively. <Pl: enclosed in plagioclase. <Ga: enclosed in garnet.

domains in Ga-I and Ga-II (selected analyses in Table 4).

The plagioclases are calcic oligoclase to sodic andesine (An_{21-31} in the matrix; An_{26-34} in the domains). This variation is due mainly to zoning; rim compositions are similar (An_{28-31}) for plagioclase from the matrix and the domains.

5.6. Corundum and sillimanite

Three corundum grains and five sillimanite prisms in the matrix were analyzed, and

Table 4. Representative microprobe analyses of plagioclase.

	M>I Pl_1		M>II Pl_2		I_1 Pl_3		II_1 Pl_4	
	C	R	C	R	C	R	C	R
Anal. No.	50	49	64	65	29	28	103	104
SiO_2	63.09	61.26	60.36	60.13	60.53	60.77	59.75	60.52
TiO_2	0.05	0.00	0.01	0.00	0.00	0.00	0.04	0.04
Al_2O_3	23.30	24.30	24.95	24.93	24.72	24.79	24.85	24.65
Cr_2O_3	0.00	0.01	0.00	0.00	0.00	0.00	0.00	0.00
FeO*	0.00	0.18	0.05	0.00	0.00	0.05	0.06	0.12
MnO	0.00	0.04	0.00	0.03	0.02	0.00	0.00	0.03
MgO	0.00	0.00	0.00	0.00	0.00	0.00	0.00	0.00
ZnO	—	—	0.00	0.00	0.00	0.03	—	—
CaO	4.57	5.91	6.73	6.37	6.23	6.25	6.59	6.70
Na_2O	9.46	8.16	8.27	8.18	8.59	8.25	8.00	8.30
K_2O	0.18	0.07	0.09	0.07	0.10	0.11	0.07	0.08
Total	100.65	99.93	100.46	99.71	100.19	100.25	99.36	100.44
				32 (O)				
Si	11.115	10.893	10.720	10.740	10.770	10.792	10.717	10.754
Al	4.839	5.093	5.223	5.248	5.184	5.189	5.254	5.163
Ti	0.007	0.000	0.001	0.000	0.000	0.000	0.005	0.005
Cr	0.000	0.001	0.000	0.000	0.000	0.000	0.000	0.000
Fe	0.000	0.027	0.007	0.000	0.000	0.007	0.009	0.018
Mn	0.000	0.006	0.000	0.005	0.003	0.000	0.000	0.005
Mg	0.000	0.000	0.000	0.000	0.000	0.000	0.000	0.000
Zn	—	—	0.000	0.000	0.000	0.004	—	—
Ca	0.863	1.126	1.281	1.219	1.188	1.189	1.267	1.276
Na	3.232	2.813	2.848	2.833	2.964	2.841	2.782	2.860
K	0.040	0.016	0.020	0.016	0.023	0.025	0.016	0.018
Or	1.0	0.4	0.5	0.4	0.5	0.6	0.4	0.4
Ab	78.2	71.1	68.6	69.6	71.0	70.1	68.4	68.9
An	20.9	28.5	30.9	30.0	28.5	29.3	31.2	30.7

* Total iron as FeO. C: core; R: rim. M>I, M>II: matrix plagioclase adjacent to Ga-I and Ga-II, respectively. I_1: domain 1 in Ga-I; II_1: domain 1 in Ga-II.

two analyses for each mineral are listed in Table 5. The only significant impurity in these minerals is Fe_2O_3 (0.51–0.63 wt% for corundum and 0.69–1.11 wt% for sillimanite).

5.7. *Ilmenite and magnetite*

Three grains of each of ilmenite (one in matrix, two included in Ga-I) and magnetite (all matrix) were analyzed. An analysis of each mineral is listed in Table 5.

The magnetites are compositionally close to the endmember with trace amounts of Cr_2O_3 (0.69–0.91 wt%).

The ilmenites probably contain Fe_2O_3, which can be estimated from stoichiometry. This, together with ferric iron in spinel, corundum and sillimanite, suggests moderately oxidizing conditions of metamorphism.

Table 5. Representative microprobe analyses of corundum, sillimanite, ilmenite and magnetite.

	Corundum		Sillimanite		Ilmenite	Magnetite
Anal. No.	Crn_1 95	Crn_2 97	Sil_1 13	Sil_2 57	Il_1 35	Mt_1 100
SiO_2	0.00	0.00	36.45	36.77	0.00	0.00
TiO_2	0.00	0.00	0.01	0.03	50.97	0.00
Al_2O_3	98.91	99.47	61.79	61.65	0.00	0.19
Cr_2O_3	0.11	0.03	0.04	0.05	0.00	0.91
Fe_2O_3	0.56*	0.51*	0.69*	0.77*	4.20**	67.84**
FeO	—	—	—	—	44.68	31.01
MnO	0.00	0.01	0.00	0.08	0.21	0.01
MgO	0.00	0.00	0.00	0.00	0.41	0.00
ZnO	0.00	0.00	0.00	—	0.07	0.10
CaO	0.00	0.00	0.01	0.00	0.01	0.01
Na_2O	0.00	0.00	0.00	0.03	0.06	0.00
K_2O	0.00	0.02	0.01	0.03	0.00	0.00
Total	99.58	100.04	99.00	99.41	100.61	100.07
	6 (O)		20 (O)		6 (O) & 4 cat.	8 (O) & 6 cat.
Si	0.000	0.000	3.984	4.005	0.000	0.000
Al	3.983	3.986	7.960	7.915	0.000	0.017
Ti	0.000	0.000	0.001	0.002	1.920	0.000
Cr	0.003	0.001	0.003	0.004	0.000	0.055
Fe^{3+}	0.014	0.013	0.057	0.063	0.166**	3.928**
Fe^{2+}	—	—	—	—	1.864	1.993
Mn	0.000	0.000	0.000	0.007	0.009	0.001
Mg	0.000	0.000	0.000	0.000	0.031	0.000
Zn	0.000	0.000	0.000	—	0.003	0.006
Ca	0.000	0.000	0.001	0.000	0.001	0.001
Na	0.000	0.000	0.000	0.006	0.006	0.000
K	0.000	0.001	0.001	0.004	0.000	0.000

* Total iron. ** Calculated by normalizing to 6 oxygens and 4 cations for ilmenite and 8 oxygens and 6 cations for magnetite.

6. Interpretative Remarks

The staurolite-bearing corundum-garnet gneiss was subjected to granulite-facies metamorphism, because the gneiss is closely associated with orthopyroxene- and two-pyroxene-bearing gneisses of intermediate to basic compositions. Textural and mineralogical features of the corundum-garnet gneiss suggest that the magnesian garnet core and matrix minerals equilibrated under granulite-facies conditions, while the staurolite was isolated from the matrix minerals during the granulite-facies event.

As shown in the mineral chemistry, garnet, staurolite and spinel are poor in Ca, Mn and Ti, the former two being also poor in Zn, and sillimanite and corundum are poor in Fe_2O_3 and Cr_2O_3, so that parageneses of these minerals can be treated in the model system Al_2O_3-FeO-MgO-SiO_2-H_2O although spinel contains ZnO to some extent. The high-grade mineral association, garnet (core)-corundum-spinel (matrix)-sillimanite,

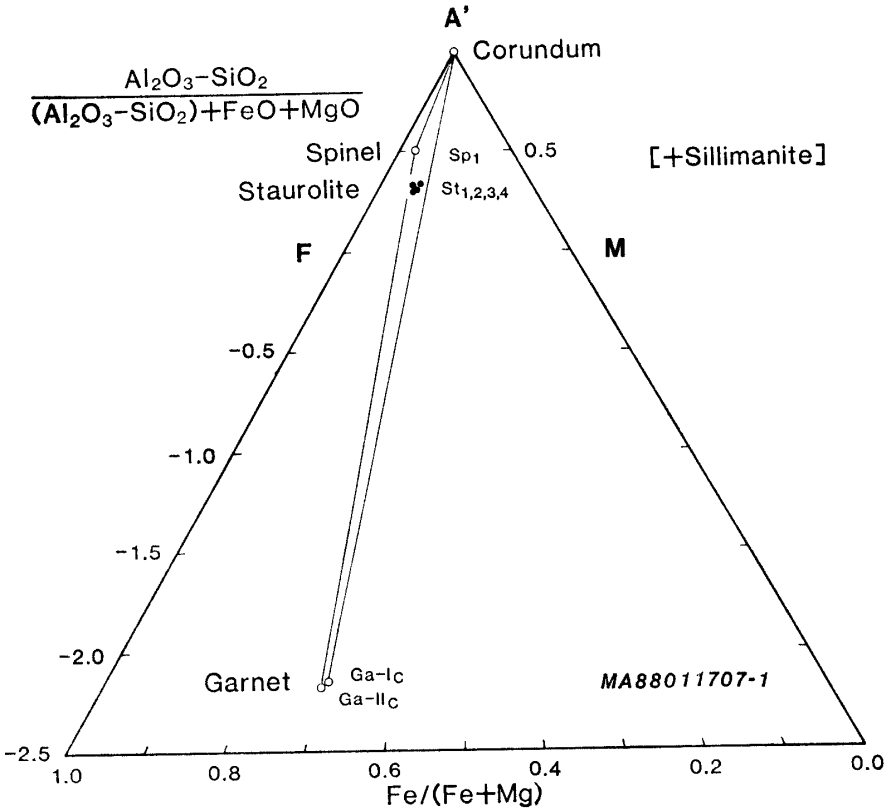

Fig. 7. A'FM diagram showing compositional relations among staurolite, corundum, garnet, spinel and sillimanite. This diagram is projected from Al_2SiO_5 onto the Al_2O_3-FeO-MgO plane of Al_2O_3-FeO-MgO-SiO_2 tetrahedron. Mineral numbers of garnet, staurolite and spinel correspond to those in Tables 1 and 2.

is illustrated together with the staurolite compositions in Fig. 7. Compositions of staurolite plot almost within the three-phase field of corundum, garnet and spinel.

In silica-undersaturated, Fe-Al-rich rocks belonging to the above system, the following univariant reaction is terminal to staurolite:

$$\text{Staurolite} = \text{Garnet} + \text{Corundum} + \text{Spinel} + \text{Sillimanite} + H_2O. \quad (1)$$

The reaction is divariant in the system with ZnO, which is more appropriate for the rock concerned. The product mineral association is the same as the granulite-facies association mentioned above. Moreover, the compositional relation shown in Fig. 7 is consistent with the reaction (1). Therefore, in the matrix of the gneiss, staurolite is considered to have been unstable during the formation of the granulite-facies mineral association. In other words, the staurolite in the domains probably is metastable relics isolated from the matrix by garnet growth during prograde metamorphism. As pointed by HIROI and KISHI (1989b), it is possible that during staurolite breakdown, the dehydration reaction (1) is obstructed by confinement of released vapor within the domains enclosed in garnet, and as a result, staurolite remains in garnet although it disappears from the matrix. Examples of the prograde staurolite-breakdown and retrograde

staurolite-formation by the reaction (1) have been reported by SCHENK (1984) and ENAMI and ZANG (1988).

The anhydrous mineral association garnet-corundum-spinel-sillimanite can be used to infer *P-T* conditions of granulite-facies metamorphism (HARRIS, 1981; BOHLEN *et al.*, 1986; DROOP and BUCHER-NURMINEN, 1984; HIROI and KISHI, 1989a, b; SCHULTERS and BOHLEN, 1989). The four minerals are related by the reaction

$$\text{Garnet} + \text{Corundum} = \text{Spinel} + \text{Sillimanite}, \qquad (2)$$

which is univariant in the Al_2O_3-FeO-SiO_2 system. The equilibrium, along with the effect of gahnite component in spinel on it, has been experimentally studied by SHULTERS and BOHLEN (1989). Using their calibration and a possible metamorphic pressure of 7 kb (GREW *et al.*, 1989), equilibrium temperatures of about 840°C are obtained from the garnet (core)-corundum-spinel (matrix)-sillimanite association in the gneiss. The values are high compared with the granulite-facies temperatures estimated at 700–750°C in this area (GREW *et al.*, 1989; MAKIMOTO *et al.*, 1990).

Garnet-biotite equilibrium temperatures were estimated for two groups of K_D values shown in Fig. 5 using several thermometries (Table 6). FERRY and SPEAR (1978) calibration for the Ti-, Ca- and Mn-free system gives unrealistically high temperatures to the garnet core-Type-A biotite pairs. Temperatures calculated for the pairs using the other calibrations, 790–980°C, are also high for the main granulite-facies metamorphism in this area. Such high temperatures may be due to the large uncertainty in the high temperature range of the garnet-biotite calibrations. On the other hand, temperatures around 630°C (560–700°C) are obtained for the Fe-Mg redistribution between contacting garnet and biotite. The values are close to temperatures estimated at 500–600°C (GREW *et al.*, 1989) and 520–670°C (MAKIMOTO *et al.*, 1990) for a later, discrete amphibolite-facies event. For further discussion on metamorphic conditions in this area, more *P-T* estimates from various rock types are required.

From the above discussion, three metamorphic episodes are distinguishable in the

Table 6. Temperature estimates from garnet and biotite compositions.

Anal. No. Ga	Bi	$\left(\frac{Mg}{Fe}\right)_{Ga}$	$\left(\frac{Mg}{Fe}\right)_{Bi}$	$\ln K_D^{Bi-Ga}$	X_{Ca}^{Ga}	X_{Mn}^{Ga}	X_{Al}^{Bi}	X_{Ti}^{Bi}	Temperature °C (at 7 kb) T	FS	PL	IM
42(C)	2(A)	0.451	0.964	0.760	0.039	0.017	0.126	0.064	979	1126	807	959
79(C)	91(A)	0.436	0.986	0.816	0.043	0.016	0.119	0.064	949	1076	791	922
20	6(A′)	0.262	1.223	1.541	0.030	0.035	0.136	0.034	663	655	616	596
19	18(A′)	0.297	1.416	1.562	0.033	0.025	0.131	0.050	657	647	612	560
69	68(A′)	0.245	1.007	1.413	0.046	0.044	0.133	0.053	704	709	642	632
17	16(B)	0.261	1.076	1.416	0.034	0.031	0.116	0.057	703	708	642	613
39	38(B)	0.383	1.707	1.494	0.037	0.015	0.102	0.041	678	674	625	605
63′	62′(B)	0.376	1.786	1.558	0.039	0.017	0.103	0.052	658	648	612	566

C: garnet core. A, A′, B: Type-A, -A′, -B. $X_i^{Ga}=i/(Fe+Mg+Mn+Ca)$. $X_i^{Bi}=i/(Fe+Mg+Mn+Al^{VI}+Ti)$. T: THOMPSON (1976), FS: FERRY and SPEAR (1978), PL: PERCHUK and LAVRENT'EVA (1983), IM: INDARES and MARTIGNOLE (1985). Analytical numbers correspond to those in Tables 1 and 2.

staurolite-bearing gneiss: (1) an earlier recrystallization, represented by the staurolite relics, in a prograde process, (2) the main granulite-facies metamorphism, and (3) a later, lower-temperature event suggested by the Fe-Mg redistribution between contacting garnet and biotite (Fig. 5). In this area, kyanite relics have been found as shown in Fig. 2 and their occurrences imply a medium pressure-type prograde *P-T-t* path attaining the granulite-facies conditions. In addition, a later, discrete amphibolite-facies event has been recognized (ASAMI *et al.*, 1989; GREW, *et al.*, 1989; MAKIMOTO *et al.*, 1990). The episodes (1) to (3) are well consistent with these regional metamorphic histories.

Acknowledgments

We wish to express our sincere thanks to the other members of the Sør Rondane survey party of JARE-29 for their kind support during the field work. We are grateful to Drs. H. KOJIMA and Y. MOTOYOSHI of the National Institute of Polar Research for their practical assistance with microprobe analyses. One (M.A.) of us would like to thank Prof. T. NUREKI of Okayama University for full facilities for this study and to Dr. HIROI of Chiba University for the valuable petrological information. His thanks are also due to Miss K. SHIMAOKA of Okayama University for preparing thin sections and the manuscript. GREW's research was funded by U.S. National Science Foundation grant DPP8613241 to the University of Maine.

References

ALBEE, A. L. (1972): Metamorphism of pelitic schists; Reaction relations of chloritoid and staurolite. Bull. Geol. Soc. Am., **83**, 3249–3268.

ASAMI, M., MAKIMOTO, H. and GREW, E. S. (1989): Geology of the eastern Sør Rondane Mountains, East Antarctica. Proc. NIPR Symp. Antarct. Geosci., **3**, 81–99.

ASHWORTH, J. R. (1975): Staurolite at anomalously high grade. Contrib. Mineral. Petrol., **53**, 281–291.

BALLEVRE, M., PINARDON, J. L., KIENAST, J. R. and VUICHARD, J. P. (1989): Reversal of Fe-Mg partitioning between garnet and staurolite in eclogite-facies metapelites from the Champtoceaux nappe (Brittany, France). J. Petrol., **30**, 1321–1349.

BOHLEN, S. R., DOLLASE, W. A. and WALL, V. J. (1986): Calibration and applications of spinel equilibria in the system FeO-Al_2O_3-SiO_2. J. Petrol., **27**, 1143–1156.

DEER, W. A., HOWIE, R. A. and ZUSSMAN, J. (1982): Rock-forming Minerals, Vol. 1A: Orthosilicates. 2nd ed. London, Longman, 919 p.

DROOP, T. R. and BUCHER-NURMINEN, K. (1984): Reaction textures and metamorphic evolution of sapphirine-bearing granulites from the Gruf Complex, Italian Central Alps. J. Petrol., **25**, 766–803.

ENAMI, M. and ZANG, Q. (1988): Magnesian staurolite in garnet-corundum rocks and eclogite from the Donghai district, Jiangsu province, east China. Am. Mineral., **73**, 48–56.

FERRY, J. M. and SPEAR, F. S. (1978): Experimental calibration of the partitioning of Fe and Mg between biotite and garnet. Contrib. Mineral. Petrol., **66**, 113–117.

GANGULY, J. (1972): Staurolite stability and related parageneses; Theory, experiments, and applications. J. Petrol., **13**, 335–365.

GREW, E. S. and SANDIFORD, M. (1985): Staurolite in a garnet-hornblende-biotite schist from the Lanterman Range, northern Victoria Land, Antarctica. Neues Jahrb. Mineral. Monatshe., **9**. 396–410.

GREW, E. S., ASAMI, M. and MAKIMOTO, H. (1988): Field studies in the eastern Sør Rondane Mountains, East Antarctica, with the 29th Japanese Antarctic Research Expedition (JARE). Antarct. J. U. S., **23**(5), 44–46.

GREW, E. S., ASAMI, M. and MAKIMOTO, H. (1989): Preliminary petrological studies of the metamorphic rocks of the eastern Sør Rondane Mountains. Proc. NIPR Symp. Antarct. Geosci., **3**, 100–127.

GUIDOTTI, C. V. (1984): Micas in metamorphic rocks. Reviews in Mineralogy, Vol. 13, Micas, ed. by S. W. BAILEY. Washington, Mineralogical Society of America, 357–467.

GUIDOTTI, C. V., CHENEY, J. T. and GUGGENHEIM, S. (1977): Distribution of titanium between coexisting muscovite and biotite in pelitic schists from northwestern Maine. Am. Mineral., **62**, 438–448.

HARRIS, N. (1981): The application of spinel-bearing metapelites to *P/T* determinations; An example from South India. Contrib. Mineral. Petrol., **76**, 229–233.

HIROI, Y. (1987): Fe-Mg-Zn jûjiseki koyôtai ni tsuite (Fe-Mg-Zn staurolite solid solution). Ganseki Kôbutsu Koshô Gakkaishi (J. Mineral. Petrol. Econ. Geol.), **82**, 160–161 (abstract).

HIROI, Y. and KISHI, S. (1989a): *P-T* evolution of Abukuma metamorphic rocks in north-east Japan; Metamorphic evidence for oceanic crust obduction. Evolution of Metamorphic Belts, ed. by J. S. DALY *et al.* Oxford, Blackwell, 481–486 (Geological Society Special Publication No. 43).

HIROI, Y. and KISHI, S. (1989b): Abukuma henseitai, Takanuki deishitsu henmagan-chû no jûjiseki to ranshôseki (Staurolite and kyanite in the Takanuki pelitic genisses of the Abukuma metamorphic terrane, northeast Japan). Ganseki Kôbutsu Koshô Gakkaishi (J. Mineral. Petrol. Econ. Geol.), **84**, 141–151.

HIROI, Y., SHIRAISHI, K., YANAI, K. and KIZAKI, K. (1983): Aluminum silicates in the Prince Olav and Sôya Coasts, East Antarctica. Mem. Natl Inst. Polar Res., Spec. Issue, **28**, 115–131.

HOSCHEK, G. (1969): The stability of staurolite and chloritoid and their significance in metamorphism of pelitic rocks. Contrib. Mineral. Petrol., **22**, 208–232.

INDARES, A. and MARTIGNOLE, J. (1985): Biotite-garnet geothermometry in the granulite facies; The influence of Ti and Al in biotite. Am. Mineral., **70**, 272–278.

MAKIMOTO, H., ASAMI, M. and GREW, E. S. (1990): Metamorphic conditions of ultramafic lenses from the eastern Sør Rondane Mountains, East Antarctica. Proc. NIPR Symp. Antarct. Geosci., **4**, 9–21.

MOTOYOSHI, Y. (1986): Prograde and progressive metamorphism of the granulite-facies Lützow-Holm Bay region, East Antarctica. D. Sc. thesis, Hokkaido Univ., 238 p.

MOTOYOSHI, Y., MATSUBARA, S., MATSUEDA, H. and MATSUMOTO, Y. (1985): Garnet-sillimanite gneisses from the Lützow-Holm Bay region, East Antarctica. Mem. Natl Inst. Polar Res., Spec. Issue, **37**, 82–94.

PERCHUK, L. L. and LAVRENT'EVA, I. V. (1983): Experimental investigation of exchange equilibria in the system cordierite-garnet-biotite. Kinetics and Equilibrium in Mineral Reactions, ed. by S. SAXENA. New York, Springer, 199–239.

RAO, B. B. and JOHANNES, W. (1979): Further data on the stability of staurolite + quartz and related assemblages. Neues Jahrb. Mineral. Monatshe., **10**, 437–447.

RICE, J. M. (1985): Experimental partitioning of Fe and Mg between coexisting staurolite and garnet. EOS, **66**, 1127 (abstract).

RICHARDSON, S. W. (1968): Staurolite stability in a part of the system Fe-Al-Si-O-H. J. Petrol., **9**, 476–488.

SCHENK, V. (1984): Petrology of felsic granulites, metapelites, metabasics, ultramafics, and metacarbonates from Southern Calabria (Italy); Prograde metamorphism, uplift and cooling of a former lower crust. J. Petrol., **25**, 255–298.

SHIRAISHI, K. (1986): Geology and petrology of Late Proterozoic metamorphic complexes in eastern Queen Maud Land, East Antarctic shield. D. Sc. thesis, Hokkaido Univ., 246 p.

SHULTERS, J. C. and BOHLEN, S. R. (1989): The stability of hercynite and hercynite-gahnite spinels in corundum- or quartz-bearing assemblages. J. Petrol., **30**, 1017–1031.

THOMPSON, A. B. (1976): Mineral reactions in pelitic rocks; II. Calculation of some P-T-X (Fe-Mg)

phase relations. Am. J. Sci., **276**, 425–454.
VAN AUTENBOER, T. (1969): Geology of the Sør-Rondane Mountains. Geologic Maps of Antarctica, ed. by C. CRADDOCK *et al.* New York, Am. Geogr. Soc., Pl. VIII (Antarct. Map Folio Ser., Folio 12, ed. by V. C. BUSHNELL).

(Received April 9, 1990; Revised manuscript received May 16, 1990)